Synthesis and Multitopic Complex Formation of a Photochromic Bis(crown ether) Based on Benzobis(thiazole)

Yu. V. Fedorov,[†] O. Fedorova,*[,†] N. Schepel,[†] M. Alfimov,[†] A. M. Turek,[‡] and J. Saltiel*[,§]

Photochemistry Center of Russian Academy of Sciences, Novatorov str., 7a, 119421, Moscow, Russia, Department of Chemistry and Biochemistry, The Florida State University, Tallahassee, Florida 32306-4390, and Faculty of Chemistry, Jagiellonian University, 30 060 Cracow, Poland

Received: March 24, 2005; In Final Form: August 1, 2005

2,7-Bis[2-(6,7,9,10,12,13,15,16-octahydro-5,8,11,14,17-pentaoxabenzocyclopentadecen-2-yl)vinyl]-benzo-[1,2-*d*;3,4-*d*′]bisthiazole, **2**, with crown ether styryl moieties substituted on a heterocyclic core, was synthesized and its complex forming ability with several metal cations was evaluated in acetonitrile by absorption and fluorescence spectroscopy. The results are compared to those for the analogous ligand possessing a single crown ether styryl moiety. Selective binding of the metal cation at the heterocyclic core of both ligands was observed only for Hg^{2+}. Alkali and alkaline earth cations bind selectively at the crown ether moieties. Stability constants and pure spectra of defined stoichiometry were determined with the use of HYPERQUAD, a least-squares fitting program, and the results were validated in one case by subjecting the titration spectral matrix to singular value decomposition with self-modeling (SVD-SM). The multitopic ligand **2** forms relatively strong 2:2 stoichiometric complexes with K^+, among the alkali metal cations, and Ba^{2+}, among the alkaline earth metal cations, and is a promising selective optical sensor for these ions.

Introduction

Compounds composed of a photochromic unit bearing a crown-ether substituent are potentially useful as selective optical sensors for metal cations.[1−5] Substantially altered photochemical and photophysical properties of complexes with metal cations provide the means for their detection.

We recently described the synthesis and complex forming behavior of the crown-containing 2-styrylbenzothiazole **1**.[6−8] Various metal cations were shown to bind with **1** through the participation of two binding centers in the dye molecule, the crown ether moiety, and the heterocyclic chromophore. The two binding centers exhibit different selectivity for metal cations, which is reflected in different optical responses on complexation at each binding site. As an extension of this work, we describe the synthesis and complex forming behavior of **2**, a bis(crown ether) with a central benzobis(thiazole) core (Scheme 1).

Earlier studies of a number of bis(crown ether) derivatives have established that they generally exhibit larger stability constants and higher metal cation binding selectivity than corresponding mono-crown ethers.[9−12] Notable is their use in distinguishing between achiral and chiral primary bisammonium salts.[13,14] Relevant to our work are reports on photochromic groups that are covalently flanked by two crown ether moieties.[15−18] Light absorption by such molecules triggers their photochromic response and results in modulation of their affinity for cations.

Compound **2**, the focus of this investigation, affords two crown ether binding sites but can also bind metal cations at the central heterocyclic moiety. We compare the complexing behavior of **1** and **2** and report on the metal cation selectivity and specificity of complex formation at different binding centers of **2**. This bis(crown ether) has the potential of serving as an optical sensor because it selectively forms stable complexes with large cations.

SCHEME 1

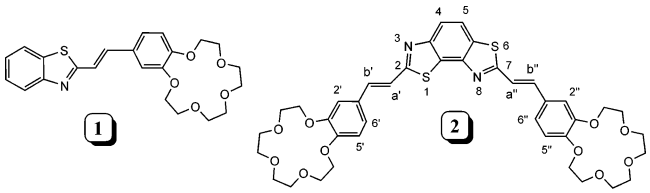

Experimental Section

Materials. Unless otherwise indicated, reagents and solvents were obtained from commercial sources and were used as received. Perchlorates of Mg, Ca, Ba, Na, K, Rb, and Cs were dried in vacuo at 230 °C. Spectroscopic grade acetonitrile containing <0.005% water was used as received.

Synthesis and Characterization. Melting points were determined with a MEL-Temp II apparatus in capillary tubes and are uncorrected. 1D ^{1}H NMR spectra were recorded on a Bruker DRX500 instrument (500.13 MHz) with CD_3CN as solvent and internal reference (1.96 ppm for ^{1}H) or with $(CD_3)_2SO$ as solvent; 2D homonuclear NOESY spectra were used to assign proton and carbon signals (the usual abbreviations designate signal multiplicities in ^{1}H NMR spectra: s, singlet; d, doublet; t, triplet; m, multiplet; dd, doublet of doublets). Mass spectra were measured at an ionizing voltage of 70 eV by electron impact with a Finnigan MAT 8430 spectrometer. Elemental analyses were performed at the microanalytical laboratory of the A. N. Nesmeyanov Institute of Organoelemental Compounds, Moscow, Russia. The course of the reactions was monitored by TLC on Merck DC-Alufolien aluminum oxide 60 F_{254} neutral (Typ E) and Kieselgel 60 F_{254} plates.

* To whom correspondence should be addressed.
[†] Photochemistry Center of Russian Academy of Sciences.
[‡] Jagiellonian University.
[§] The Florida State University.

10.1021/jp0515333 CCC: $30.25
Published on Web 09/07/2005

Potassium *tert*-butoxide (*t*-BuOK) was prepared by dissolution of the alkali metal in anhydrous *t*-BuOH, evaporation of excess alcohol, and drying of the salt in vacuo. Preparations of *N*-(3-acetylaminophenyl)acetamide, *N*-(3-thioacetylaminophenyl)acetamide, and 2,7-dimethylbenzo[1,2-*d*,3,4-*d*′]bisthiazole were as described earlier.[19,20]

2,7-Bis[2-(6,7,9,10,12,13,15,16-octahydro-5,8,11,14,17-pentaoxabenzocyclopentadecen-2-yl)vinyl]benzo[1,2-*d*;3,4-*d*′]-bisthiazole (2). A mixture of 44 mg of **3** (0.2 mmol), 130 mg of 4′-formylbenzo-15-crown-5 ether (0.44 mmol), and 49 mg of *t*-BuOK (0.44 mmol) in 10 mL of anhydrous dimethylformamide (DMF) was kept at ambient temperature for 24 h. Distilled water (20 mL) was added to precipitate the product, which was filtered and crystallized from CH_3CN. The yield of **2** was 280 mg (18%); mp 162 °C. ^{1}H NMR (500 MHz, CD_3CN, 30 °C) δ 3.6 (m, 16 H, 8 CH_2O), 3.95 (m, 8 H, 4 CH_2O), 4.50 (m, 8 H, 4 CH_2O), 7.01 (d, 2 H, H-5′, H-5″, $J = 8.5$ Hz), 7.31−7.33 (2d, 2H, H-6′, H-6″, $J = 8.5$ Hz), 7.46 and 7.49 (2s, 2 H, H-2′, H-2″), 7.58 (d, $J = 16.1$ Hz, 1 H, H-a), 7.66 (s, 2 H, H-a, H-b), 7.69 (d, $J = 16.1$ Hz, 1 H, H-b), 7.92 (d, 1 H, H-5, $J = 8.6$ Hz), 8.18 (d, 1 H, H-4, $J = 8.6$ Hz). MS (EI, 70 eV) *m*/*z* 776 (100), 500 (87), 224 (13), 184(14), 144 (24), 125 (21), 114 (20), 77 (15), 63 (13), 58 (45), 51 (27). Calcd for $C_{40}H_{44}N_2O_{10}S_2$: C 61.84, H 5.71, N 3.61. Found: C 61.74, H 5.84, N 3.61.

Spectroscopic Measurements. UV−vis spectra were recorded with the use of a Specord-M40 spectrophotometer. Solution preparations and measurements were carried out in red light. Steady-state fluorescence spectra were recorded with a Shimadzu RF-5000 fluorescence spectrophotometer, or with a Hitachi F4500 fluorimeter. In a few cases, fluorescence spectra were recorded for both air-saturated and Ar-bubbled acetonitrile (AN) solutions. Fluorescence quantum yields of the ligands and their complexes were determined at 20 ± 1 °C in standard 1-cm^2 quartz cells with air-saturated AN relative to quinine sulfate in 0.5 M H_2SO_4 as a standard ($\phi_F = 0.55$)[21,22] with excitation at 365 nm. Quantum yields are based on areas of fluorescence spectra uncorrected for nonlinearity in instrumental response.

Equilibrium Constant Determination. Complex formation of **2** with $Mg(ClO_4)_2$, $Ca(ClO_4)_2$, $Ba(ClO_4)_2$, $Hg(ClO_4)_2$, $NaClO_4$, $KClO_4$, $RbClO_4$, or $HClO_4$ in acetonitrile at 20 ± 1 °C was studied by spectrophotometric titration. The ratio of **2** to $Mg(ClO_4)_2$, $Ca(ClO_4)_2$, $Ba(ClO_4)_2$, $Hg(ClO_4)_2$, $NaClO_4$, $KClO_4$, $RbClO_4$, or $HClO_4$ was varied by adding aliquots of a solution containing known concentrations of **2** and of corresponding salt or acid to a solution of **2** alone of the same concentration. The absorption spectrum of each solution was recorded and the stability constants of the complexes were determined using the HYPERQUAD program,[23a] as described in our earlier work.[23b,c] In simple cases involving formation of a single complex, mixture compositions were obtained from titration curves. HYPERQUAD was used when more than a single complex formed. Formation of complexes of various stoichiometries was evaluated and, as a rule, complexes that were predicted to contribute less than 5% of the total ligand concentration were eliminated from consideration.

Data Analysis. SVD-SM calculations were performed on a Dell computer working with appropriate routines in the environment of MATLAB packages, versions 5.2 and 6.1.

Results and Discussion

Synthesis. The bisheterocyclic compound 2,5-dimethylbenzobis(thiazole) **3** was obtained in three steps as described earlier.[19,20] The target compound **2** was prepared by condensation of **3** with 4′-formyl-2,3-benzo-15-crown-5 ether in the presence of *t*-BuOK in DMF at ambient temperature (Scheme 2).

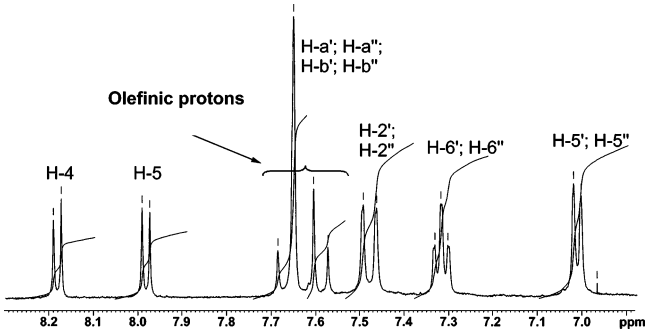

Figure 1. Aromatic and olefinic region of the ^{1}H NMR spectrum of **2** in DMSO-d_6, 25 °C, 500 Hz.

SCHEME 2

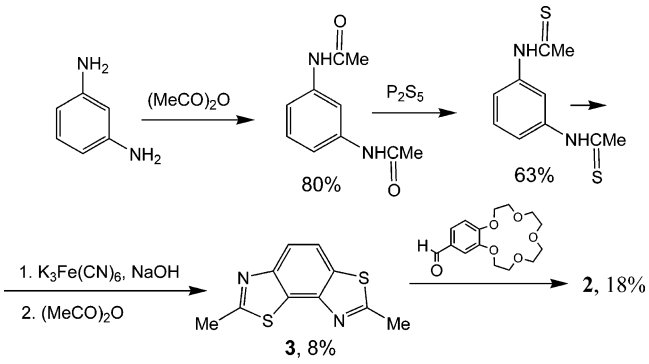

Structural assignment to **2** is based, in part, on its ^{1}H NMR spectrum (Figure 1). Differences in the chemical shifts of the four proton pairs H-6′ and H-6″, H-2′ and H-2″, H-a′ and H-a″, and H-b′ and H-b″ are consistent with the unsymmetrical nature of the central heterocyclic core. We can assign the *E* configurations to one of the double bonds whose protons appear as a doublet of doublets with $J = 16.1$ Hz (CD_3CN). The protons of the other double bond appear as a singlet due to accidental coincidence of their chemical shifts and, absent the coupling constant, the ^{1}H NMR spectrum does not reveal that double bond's stereochemistry. We assign it the *E* stereochemistry on the basis of UV−vis observations (see below).

UV−Vis Spectroscopic Observations. The electronic absorption spectrum of **2** in CH_3CN is characterized by an intense long wavelength absorption band (LAB) with λ_{max} at 374 nm (ϵ_{trans} 62 600 cm^{-1} M^{-1}) (Figure 2). The more extensive conjugation in **2** shifts its LAB bathochromically relative to that of the monostyrylcrown ether analogue **1**. Such shifts for bischromophoric compounds have been reported previously.[19] The molar absorptivities of **2** are close to double those of **1**, consistent with assignment of the *E* configuration to both double bonds. Photochemical observations showing that pronounced absorbance attenuation accompanies sequential $E \rightarrow Z$ photoisomerization steps support this assignment.[24]

Additions of perchlorates of alkali or alkaline earth metal ions (Na, K, Rb, Mg, Ca, Ba) to solutions of **2** in CH_3CN (2.4×10^{-5} M) lead to hypsochromic shifts in the LAB signaling the expected formation of complexes between these ions and the crown ether moieties of **2**. The LAB in **2** involves displacement of electron density from the benzene ring to the heterocyclic moiety. Binding of cations in the crown ether moieties of **2** diminishes this effect, accounting for the hypsochromic shifts of the LAB. As expected, complexation of **2** with

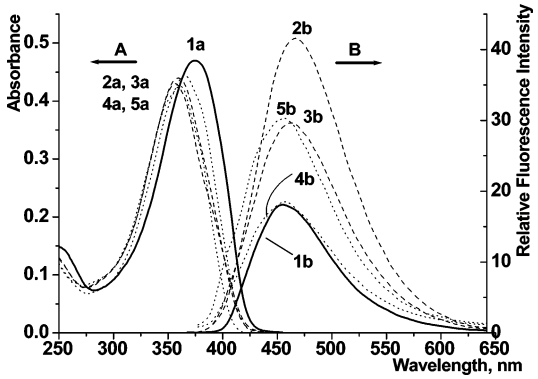

Figure 2. Absorption (A) and fluorescence (B) spectra in acetonitrile designated as a and b, respectively, of **2** (0.75×10^{-5} M) as free ligand (1a,b) and in the presence of $[Ba^{2+}] = 1.6 \times 10^{-4}$ M (2a,b), $[Ba^{2+}] = 6 \times 10^{-2}$ M (3a,b), $[Mg^{2+}] = 2 \times 10^{-5}$ M (4a,b) and $[Mg^{2+}] = 2.8 \times 10^{-3}$ M (5a,b).

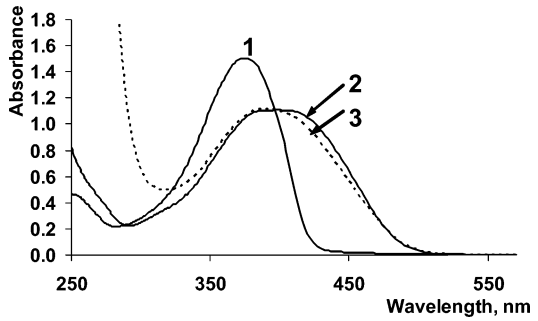

Figure 3. Absorption spectra of **2** (2.4×10^{-5} M) as free ligand (1) and in the presence of $[Hg^{2+}] = 1.3 \times 10^{-3}$ M (2) and $[Hg^{2+}] = 2.9 \times 10^{-1}$ M (3) in acetonitrile.

the doubly charged alkaline earth metal cations causes larger LAB hypsochromic shifts than complexation with the singly charged alkali metal cations. In contrast, addition of the same concentration of $Hg(ClO_4)_2$ or $HClO_4$ results in bathochromic shifts of the LAB of **2**, which we associate with formation of coordination bonds to the nitrogen atoms of the heterocyclic moiety. The sulfur atoms may also be involved in the case of Hg^{2+}. The increased positive charge in the heterocyclic core enhances its electron acceptor properties and facilitates the displacement of electron density from the benzene ring to the heterocyclic moiety lowering the transition energy associated with the LAB of **2**. A hypsochromic shift of the LAB, observed at sufficiently high concentrations of Hg^{2+}, Figure 3, suggests subsequent Hg^{2+} complex formation with the crown ether moieties of **2**. Although not firmly established by present data, we tentatively propose a 1:3 ligand to metal, **2·(Hg^{2+})$_3$**, stoichiometry for this complex.

Equilibrium Constant Determinations. Complex formation of **2** with alkali (Na^+, K^+, Cs^+, Rb^+) and alkaline earth (Mg^{2+}, Ca^{2+}, Ba^{2+}) metal cations and with $Hg(ClO_4)_2$ and $HClO_4$ was studied by spectrophotometric titration as described recently for **1**.[8] The ratio of **2** to metal cations was varied by adding aliquots of a solution containing known concentrations of **2** and of metal cations to a solution of **2** alone of the same concentration. The absorption spectrum of each solution was recorded and the stability constants of the complexes were determined using HYPERQUAD,[23] a program designed to extract equilibrium constants from potentiometric and/or spectrophotometric titration data. HYPERQUAD starts with an assumed complex formation scheme and uses a least-squares approach to derive the spectra of the complexes and the stability constants. An alternative, more powerful approach to the derivation of pure component spectra from spectral matrixes of mixture spectra is singular value decomposition with self-modeling (SVD-SM).[25] Because HYPERQUAD derived stability constants are associated with surprisingly small uncertainties, we evaluated the results from this program with a parallel SVD-SM calculation. The spectral set from ref 8 involving the titration of **1** with Ba^{2+} ions was used for this comparison.

SVD-SM Evaluation of HYPERQUAD Results for the 1/Ba^{2+} System. Stability constants for this system from ref 8 are shown in Table 1. They were derived with HYPERQUAD based on the assumption of sequential 2:1 (**1$_2$·Ba^{2+}**) and 1:1 (**1·Ba^{2+}**) complex formation with increasing Ba^{2+} concentration (equilibria 1 and 2 and Scheme 3).

$$2L + M \overset{K_{21}}{\rightleftharpoons} L_2M \quad (1)$$

$$L + M \overset{K_{11}}{\rightleftharpoons} LM \quad (2)$$

SVD analysis of the spectral matrix composed of the spectrum of **1** and spectra of **1** in the presence of 13 different Ba^{2+} concentrations in acetonitrile reveals a robust 3-component system. The possible contribution of a fourth minor component

TABLE 1: Stability Constants of Complexes 1 and 2 with Metal Cations in CH_3CN (293 K)[a]

			stability constants			
complex	cation *d*, Å	ionic strength, M	log K_{11}	log K_{12}	log K_{22}	log K_{21}
2+Ba^{2+}	2.68	$0-(1.7 \times 10^{-4})$, $(1.7 \times 10^{-4})-0.86$		7.68 (65)	17.11 (7)	
1+Ba^{2+}		0−0.2	4.7 (1)			10.8 (2)
2+Ca^{2+}	1.98	0−0.155	4.66 (4)	8.07 (11)		
1+Ca^{2+}		$0-(2.5 \times 10^{-3})$	5.6 (1)			10.3 (2)
2+Mg^{2+}	1.32	$0-(1 \times 10^{-2})$	5.64 (20)	10.15 (20)		
1+Mg^{2+}		$0-(2.5 \times 10^{-3})$	5.5 (1)			
2+Rb^+	2.96	$0-(2.5 \times 10^{-3})$		8.68 (40)	14.08 (46)	
2+K^+	2.66	$0-(1.67 \times 10^{-4})$			15.97 (84)	
2+Na^+	1.9	$0-(3 \times 10^{-3})$	4.94 (97)	8.44 (11)		
2+H^+		0−0.14	4.88 (14)	6.56 (62)	-	
1+H^+		$0-(2.5 \times 10^{-3})$	6.4 (5)			
2+Hg^{2+}		0−0.024	5.72 (32)	9.68 (35)	-	
1+Hg^{2+}		0−0.024	5.6 (1)	9.40 (15)		

[a] All ions as perchlorates. Values in parentheses are HYPERQUAD derived uncertainties in the last significant figures shown, see text. Results for **1** are from ref 8.

SCHEME 3

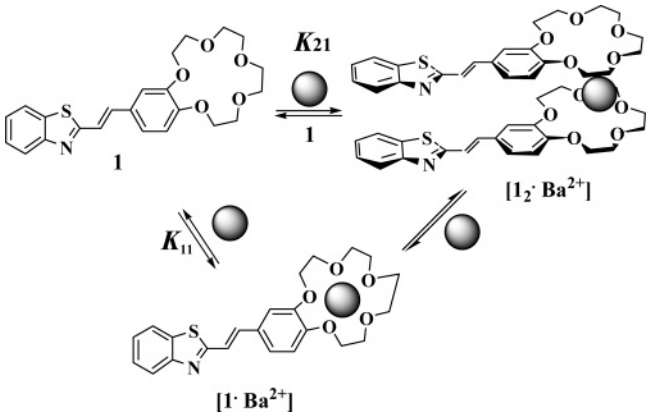

was neglected. Combination coefficient points in eigenvector space adhere closely to the stoichiometric plane (with respect to ligand concentration) defined by the three major eigenvectors. To facilitate self-modeling (SM) the points were projected to that plane, Figure 4, generating a new set of combination coefficients, which, applied to the eigenvectors, give a spectral set in excellent agreement with the experimental spectra. Since the combination coefficients of the ligand spectrum define corner 1 of the stoichiometric triangle, the task of SM is to locate the corners corresponding to the spectra of complexes $\mathbf{1}_2\cdot\mathbf{Ba}^{2+}$ and $\mathbf{1}\cdot\mathbf{Ba}^{2+}$. The initial four spectra very nearly define a 2-component system because of minimal contribution by the 1:1 complex. Because both complexes absorb to the blue of the ligand spectrum, potential $\mathbf{1}_2\cdot\mathbf{Ba}^{2+}/\mathbf{1}\cdot\mathbf{Ba}^{2+}$ sides of the triangle were located by applying the Lawton and Sylvestre (LS) nonnegativity criterion[26] to the onsets of spectra generated by moving along lines originating at corner 1 (the ligand) and passing through each of the other spectral points. Searches for the corners corresponding to the spectra of the 1:1 and 2:1 complexes on the LS line were based on minimizing the standard deviations of calculated equilibrium constant values (K_{11} and K_{21}) from mean values. The distance of the LS line from corner 1 depends on the onset spectral range on which baseline is imposed and, consequently, is somewhat arbitrary. Furthermore, whereas the location of the 2:1 complex corner is very narrowly defined in a tiny area of the stoichiometric plane, the location of the 1:1 complex corner is highly sensitive to the distance of the SL line from the ligand corner. Once the three corners in the ligand stoichiometric triangle are selected, fractional contributions with respect to ligand, x_L, x_{11} and x_{21}, are calculated and converted to mole fractions. These mole fractions and the

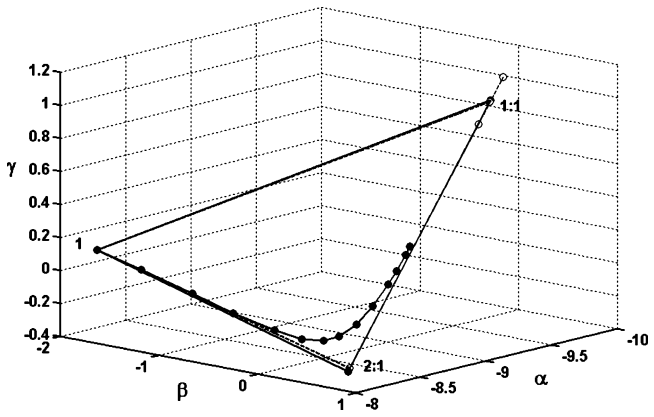

Figure 4. SVD representation of the three-component spectral system of ligand **1** and its two complexes with Ba^{2+} in eigenvector combination coefficient space.

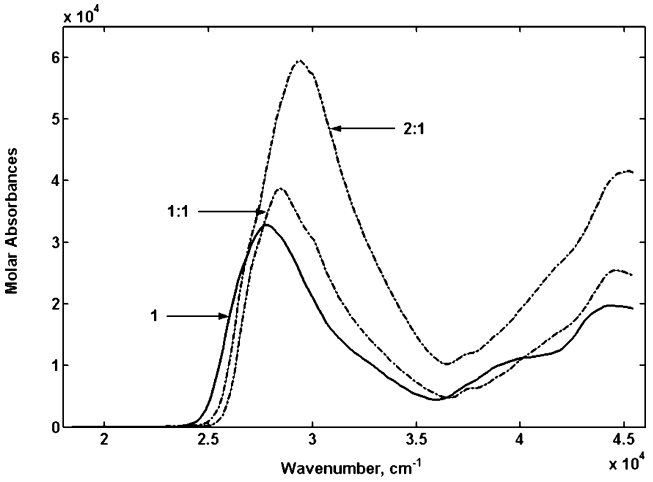

Figure 5. HYPERQUAD (- - -) and SVD-SM (—) derived spectra of the complexes with Ba^{2+} and the spectrum of **1**.

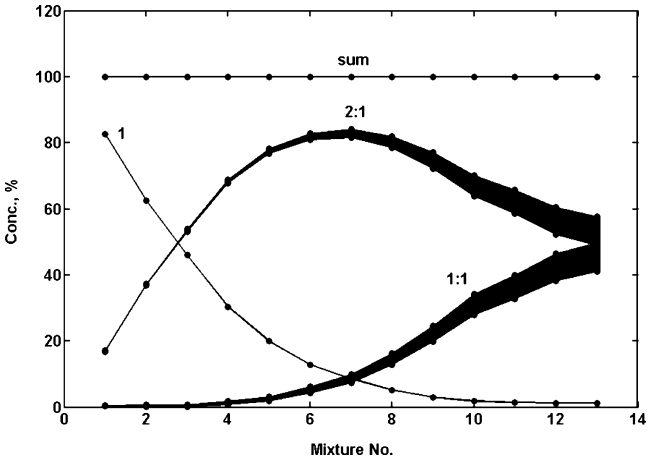

Figure 6. Changes in concentration (quantified with respect to ligand **1** contributions to the complexes) while moving the vertices for the complexes along the triangle side defined by the HYPERQUAD spectra.

corresponding equilibrium constants allow calculation of total Ba^{2+} concentrations. The distance between the SL line and corner 1 was selected by optimizing the agreement between calculated and experimental total $[Ba^{2+}]$. The final stoichiometric triangle in eigenvector combination space is shown in Figure 4. The points (open circles) close to the corners of the triangle were based on the fit of the eigenvectors to the HYPERQUAD derived spectra. Best fit combination coefficient points for the HYPERQUAD spectra deviate slightly from the stoichiometric plane whereas the SVD-SM spectra are constrained to lie in that plane. This small adjustment in the apexes of the stoichiometric triangle leads to substantial improvement in the standard deviations of K_{11} and K_{21} (log $K_{11} = 4.38 \pm 0.03$ and log $K_{21} = 10.53 \pm 0.03$) and almost imperceptible changes in the derived spectra of the two complexes, Figure 5. The ranges of the fractional contributions of the 1:1 and 2:1 complexes (in terms of ligand content) as a function of $[Ba^{2+}]$ on stepping the apex corresponding to the spectrum of the 1:1 complex in the range shown in Figure 4 (during SM) are shown in Figure 6. The fact that the fractional contributions of unbound ligand to the mixtures are not affected by changes in the length of the 1:1/2:1 side (line labeled 1 in Figure 6) of the stoichiometric triangle is important because it establishes that both SVD-SM and HYPERQUAD have accurately identified the direction of that side. The optimum concentration curves, corresponding to the pure spectra in Figure 5, are shown in

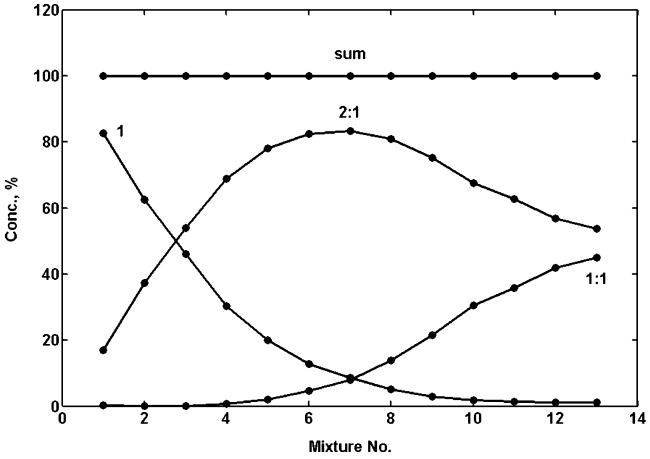

Figure 7. As in Figure 6 but based on the SVD-derived corners of the triangle in Figure 4.

Figure 7. The apparent high precision to which the equilibrium constants are given by the HYPERQUAD program (much higher than the reported[8] log $K_{11} = 4.7 \pm 0.1$ and log $K_{21} = 10.8 \pm 0.2$) is deceiving. HYPERQUAD assumes that both model (eqs 1 and 2) and reactant concentrations are exact and uses a least-squares fit to calculate the optimum concentration profile for the three components in each experimental spectrum as a function of [Ba^{2+}]. Pure component spectra are based on this concentration profile. Because the concentration profile is constrained to exactly obey eqs 1 and 2, deviations between stability constants derived from the concentrations assigned to each experimental spectrum reflect computer round-off error and are not real. Real uncertainties for the HYPERQUAD stability constants, obtained from the concentration profile generated by least-squares fitting of the HYPERQUAD pure component spectra to the experimental spectra, are significantly larger than those obtained by SVD-SM. Nevertheless, the remarkable agreement between spectra and stability constants derived by the two methods lends confidence to the use of HYPERQUAD in our work.

The 2/M^{n+} Systems. Complex formation of **2** with alkali (Na^+, K^+, Cs^+, Rb^+), alkaline earth (Mg^{2+}, Ca^{2+}, Ba^{2+}) cations, and Hg^{2+} and H^+ was studied by spectrophotometric titration. Following the procedure used for **1**, the molar ratio of **2** to the metal cation was varied by adding aliquots of a solution containing known concentrations of **2** and the metal cation (perchlorate salt) to a solution of **2** alone of the same concentration. The absorption spectrum of each solution was recorded and stability constants of the complexes were determined using HYPERQUAD. Typical absorption and fluorescence spectra are shown in Figure 8.

Four equilibria were used to model the data:

$$L + M \overset{K_{11}}{\rightleftharpoons} LM \quad (3)$$

$$L + 2M \overset{K_{12}}{\rightleftharpoons} LM_2 \quad (4)$$

$$2L + M \overset{K_{21}}{\rightleftharpoons} L_2M \quad (5)$$

$$2L + 2M \overset{K_{22}}{\rightleftharpoons} L_2M_2 \quad (6)$$

Because of the complexity associated with the availability of multiple potential sites for complex formation (Scheme 4, an oversimplification because only one of the conformers of **2** is

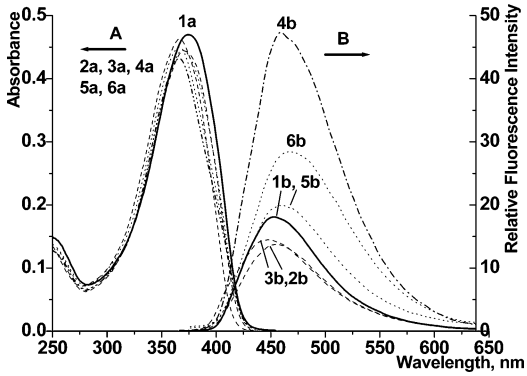

Figure 8. Absorption (A) and fluorescence (B) spectra in acetonitrile of **2** (0.75×10^{-5} M) as free ligand (1a,b) and in the presence of [Na^+] = 6.9×10^{-5} M (2a,b), [Na^+] = 6.1×10^{-3} M (3a,b), [K^+] = 1×10^{-3} M (4a,b), [Rb^+] = 6.15×10^{-5} M (5a,b), and [Rb^+] = 7.1×10^{-4} M (6a,b).

SCHEME 4

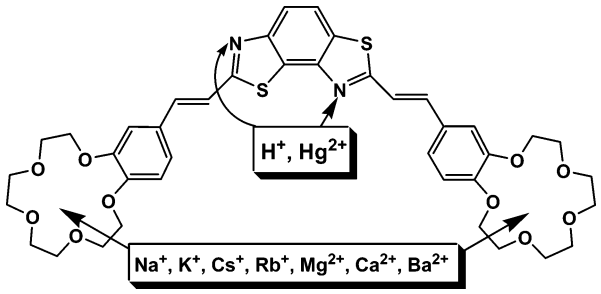

SCHEME 5

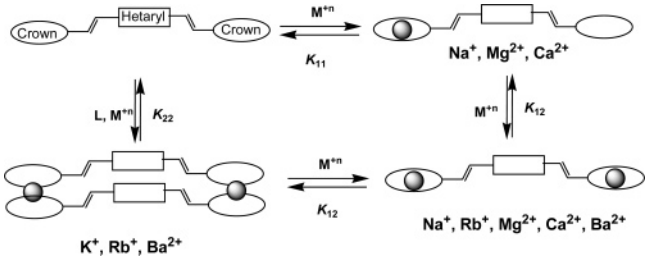

shown), HYPERQUAD fitting to stability constants was simplified by refining no more than two stability constants at a time.

The spectral sets for Na^+, Mg^{2+}, and Ca^{2+} and ligand **2** are consistent with formation of two complexes having 1:1 and 1:2 stoichiometries, namely, **2**·M^{n+} and **2**·$(M^{n+})_2$. The spectral sets for Rb^+ and Ba^{2+} in the presence of ligand **2** are consistent with formation of the 1:2 complex, **2**·$(M^{n+})_2$, but instead of a 1:1 complex they reveal formation of a 2:2 complex, $\mathbf{2}_2$·$(M^{2+})_2$. Structures for these complexes are proposed in Scheme 5 and the derived stability constants are collected in Table 1. We recognize that Scheme 5 is an oversimplification. It neglects the probable involvement of a 2:3 complex as an intermediate in the conversion of the 2:2 complex to the 1:2 complex. Formation of a 2:1 complex on the way to the 2:2 complex may also be envisioned. The simplified scheme was forced on the spectral data because analysis with HYPERQUAD becomes difficult and unreliable when there are too many species or when their concentration is very low. Preliminary SVD analysis does reveal the presence of more than 3 species. The 2:2 sandwich complex formed with Ba^{2+} is associated with the largest stability constant. HYPERQUAD derived spectra for the $\mathbf{2}_2$·$(Ba^{2+})_2$ and **2**·$(Ba^{2+})_2$ complexes are shown in Figure 9. Formation of sandwich complexes leads to a decrease in absorbance and to a hypsochromic shift of the long wavelength band. At higher

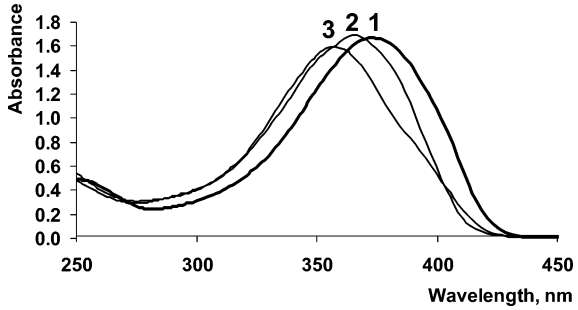

Figure 9. Absorption spectra of **2** as free ligand (1) and its complexes $\mathbf{2}\cdot(\mathbf{Ba}^{2+})_2$ (2) and $\mathbf{2}_2\cdot(\mathbf{Ba}^{2+})_2$ (3) in acetonitrile calculated from spectrophotometric titration spectral data using HYPERQUAD. $[\mathbf{2}] = [\mathbf{2}\cdot(\mathbf{Ba}^{2+})_2] = 2.4 \times 10^{-5}$ M, $[\mathbf{2}_2\cdot(\mathbf{Ba}^{2+})_2] = 1.2 \times 10^{-5}$ M.

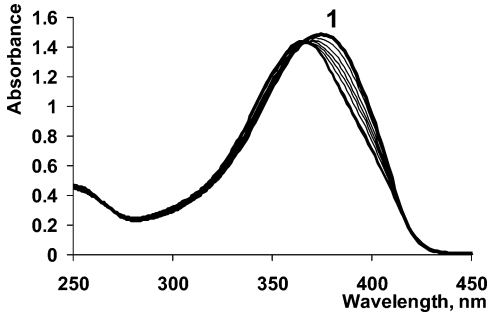

Figure 10. Absorption spectra of **2** as free ligand (1) and with increasing concentrations of $KClO_4$ in acetonitrile: $[\mathbf{2}] = 2.4 \times 10^{-5}$ M, the $[K^+]$ range is from 4.0×10^{-6} to 3.3×10^{-4} M.

$[Ba^{2+}]$ the complex composition shifts to favor formation of complex $\mathbf{2}\cdot(\mathbf{Ba}^{2+})_2$, leading to recovery of absorbance and a shift of the position of the long wavelength band toward that of the ligand. The spectrum of the 2:2 complex, Figure 9, shows subtle splitting of the long wavelength absorption band into strong and weak, short and long wavelength transitions, respectively, as expected for excitonic interaction of the transition dipole moments of the two chromophores in the sandwich complex.[27,28] The weak shoulder at the onset of the spectrum of the 2:1 complex, Figure 5, may have a similar origin. Alternatively, the development of shoulders in the absorption spectra could reflect structural heterogeneity of the complexes. The structure shown for the 2:2 complexes in Scheme 5 is arbitrary and it is not our intent to imply a conformational preference. Formation of $\mathbf{2}_2\cdot(\mathbf{Ba}^{2+})_2$ complexes reveals itself in the photochromic response of the ligand. Trans-cis photoisomerization is suppressed entirely and is replaced by sequential intramolecular cross-ligand cyclobutane ring formation yielding at least three photodimers (HPLC).[24] Multiple photodimer product formation suggests more than a single 2:2 complex structure.

Interaction of K^+ with **2**, uniquely among the alkali metal cations studied, gives only a very stable 2:2 complex. Preferential binding in the $\mathbf{2}_2\cdot(\mathbf{K}^+)_2$ sandwich complex may allow detection of K^+ in a mixture of alkali metal cations. As shown in Figure 10, except at the long wavelength onset, the absorbance of this complex is blue shifted relative to the free ligand. The isosbestic point at ~360 nm is consistent with formation of a single complex. Possibly due to the lower surface charge density of Cs^+, spectral changes accompanying complex formation with **2** (1−2 nm blue shift of the LAB) are too small to allow calculation of stability constants in this case.

The H^+/Hg^{2+} Analogy. Single and double protonations, probably at the N atoms, on addition of $HClO_4$ to an acetonitrile solution of **2** lead to pronounced successive red shifts of the

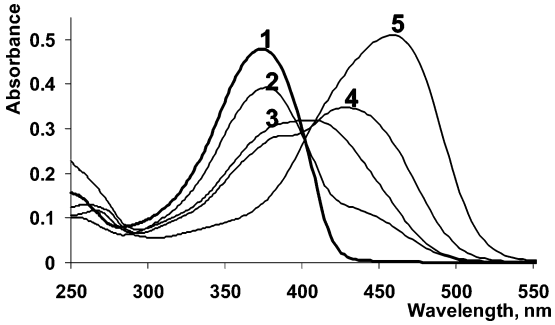

Figure 11. Absorption spectra of **2** as free ligand (1) and its complexes $\mathbf{2}\cdot\mathbf{Hg}^{2+}$ (2), $\mathbf{2}\cdot(\mathbf{Hg}^{2+})_2$ (3), $\mathbf{2}\cdot\mathbf{H}^+$ (4), and $\mathbf{2}\cdot(\mathbf{H}^+)_2$ (5) in acetonitrile calculated from spectrophotometric titration data using HYPERQUAD. $[\mathbf{2}] = [\mathbf{2}\cdot\mathbf{Hg}^{2+}] = [\mathbf{2}\cdot(\mathbf{Hg}^{2+})_2] = [\mathbf{2}\cdot\mathbf{H}^+] = [\mathbf{2}\cdot(\mathbf{H}^+)_2] = 7.5 \times 10^{-6}$ M.

SCHEME 6

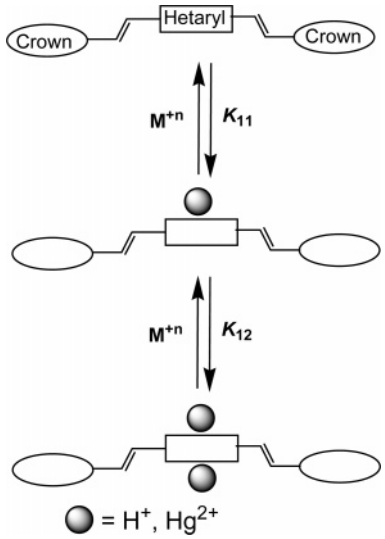

LAB that aid in the structure assignment of the complexes of **2** with Hg^{2+} (see below). HYPERQUAD derived spectra for the complexes, Figure 11, are based on the equilibria shown in Scheme 6. Nearly identical spectra for $\mathbf{2}\cdot\mathbf{H}^+$ and $\mathbf{2}\cdot(\mathbf{H}^+)_2$ to those shown in Figure 11 can be assigned to the singly and doubly protonated **2** on the basis of titrimetric curves. The spectrum of $\mathbf{2}\cdot\mathbf{H}^+$, curve 4 in Figure 11, is unusual in that it shows a pronounced shoulder in addition to a main absorption band. An attractive interpretation of this feature is that, because the N-atoms on the two sides of the central heterocyclic moiety are nearly equivalent as protonation sites, the spectrum reflects the presence of two isomeric $\mathbf{2}\cdot\mathbf{H}^+$ species.

HYPERQUAD derived spectra for 1:1 and 1:2 complexes of **2** with Hg^{2+} and corresponding stability constants are shown in Figure 11 and Table 1, respectively. In stark contrast to observations with the other cations, spectrophotometric titration of **2** with $Hg(ClO_4)_2$ is reminiscent of protonation because it is accompanied by red shifts of the LAB (albeit less pronounced). Initially, addition of $Hg(ClO_4)_2$ to the dye solution leads to a small red shift of the LAB with development of a shoulder at 450 nm signaling the formation of 1:1 complex(es) $\mathbf{2}\cdot\mathbf{Hg}^{2+}$ with binding at the central heterocyclic portion of the molecule (Scheme 6). Since, unlike protonation which should be localized at the N atoms, Hg^{2+} has strong affinities for both N and S, three binding sites can be envisioned: a central site involving coordination at S-1 and N-8, Scheme 1, and one site at each side of the heterocycle involving S-1/N-3 and S-6/N-8, respectively. Indeed, as we observed for protonation, the spectrum assigned to the 1:1 complex of **2** with Hg^{2+}, curve 2 in Figure

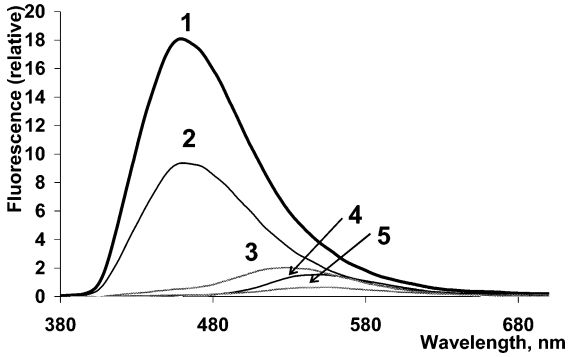

Figure 12. Fluorescence spectra of **2** alone (1) ([**2**] = 7.5×10^{-6} M) and in the presence of Hg^{2+} (2, $[Hg^{2+}] = 1.4 \times 10^{-5}$ M; 3, $[Hg^{2+}] = 3.3 \times 10^{-3}$ M) and H^+ (4, $[H^+] = 8.2 \times 10^{-4}$ M; 5, $[H^+] = 2.3 \times 10^{-2}$ M).

11, also shows a shoulder in addition to the main absorption band, suggesting that here, too, there is an equilibrium between at least two isomeric 1:1 complexes. At higher $[Hg^{2+}]$, formation of a **2·(Hg^{2+})$_2$** complex is revealed by a more pronounced bathochromic shift of the LAB suggesting that the second Hg^{2+} cation also binds at the heterocyclic moiety. An attractive structure for the 2:2 complex in Scheme 6 would have one Hg^{2+} cation bound at N-3 and S-1 and the other at N-8 and S-6. Sharing of the positive charge by S/N atom pairs may account for smaller LAB red shifts than for protonation for which positive charge is borne primarily by the N atoms.

Preferential complex formation of the heterocyclic portion of the molecule with Hg^{2+} was expected because results for the **1**/Hg^{2+} system had led to the same conclusion.[8] Indeed, examination of the stability constants in Table 1 shows that, for Hg^{2+}, log K_{11} values are nearly identical for **1** and **2**. The absence of enhanced binding between Hg^{2+} and **2** suggests that participation of the S-1/N-8 binding site in 1:1 complex formation may not be significant.

Fluorescence Measurements. The high photoreactivity of **2** is evident in the loss of intensity in successively recorded fluorescence spectra of dilute AN solutions (e.g., 7×10^{-6} M). Photochemical conversions in the course of recording spectra were minimized by using larger concentrations after demonstrating the absence of aggregation (no spectral changes and good adherence to Beer−Lambert law in the 10^{-6}−(7.4×10^{-5}) M range). Fluorescence spectra of solutions of **2** in AN in the absence and presence of metal cations or a proton source are shown in Figures 2, 8, and 12. The spectra are broad and featureless. The fluorescence spectrum of free **2**, $\lambda^{fl}_{max} = 461$ nm, is independent of oxygen concentration (no intensity changes between Ar and O_2 outgassed solutions) and undergoes small shifts in the 452−475 nm wavelength range on complexation with alkali and alkaline earth metal cations. Consistent with the absorption spectra, much larger λ^{fl}_{max} red shifts to the 530−549 nm range result on protonation and on coordination with Hg^{2+}. Fluorescence intensities are much weaker for the latter red-shifted spectra (Figure 12). For example, in the presence of $[Hg^{2+}] = 1.4 \times 10^{-5}$ M (curve 2 in Figure 12), the emission of the complex is barely discerned as a shoulder at the red tail of the spectrum. Specific λ_{max} values for absorption and fluorescence spectra are given in Table 2. Under air-saturated conditions, fluorescence quantum yields are low but generally increase on alkali and alkaline earth metal cation complexation at the crown ether moieties of both **1** and **2**, Table 2. Only in the case of protonation and complexation with Hg^{2+} is there a pronounced decrease in the fluorescence quantum yield and a significant bathochromic shift in the fluorescence spectra.

TABLE 2: Spectral Characteristics of 2 and Its Complexes in ACN at 293 K

compd	λ^{abs}_{max}/nm ($\epsilon \times 10^{-4}$)[a]	λ^{fl}_{max}/nm ($\Delta\lambda$, nm)[b]	φ_f[c]
2	374.5 (6.26)	461	0.011
1	359.2 (3.36)	452	0.0069
2·Mg^{2+}	365.0 (5.92)	461 (0)	0.013
2·Mg$^{2+}_2$	361.0 (5.68)	460 (−1)	0.022
2$_2$·Ba$^{2+}_2$	356.0 (5.73)	472 (11)	0.034
2·Ba$^{2+}_2$	359.7 (5.86)	468 (7)	0.025
2·Ca^{2+}	363.6 (5.86)	462 (1)	0.016
2·Ca$^{2+}_2$	361.6 (6.04)	461 (0)	0.022
2·Na$^+$	370.0 (5.92)	461 (0)	0.011
2·Na$^+_2$	366.3 (6.18)	452 (−9)	0.014
2$_2$·K$^+_2$	365.5 (5.76)	467 (6)	0.033
2$_2$·Rb$^+_2$	370.4 (5.93)	467 (6)	0.018
2·Rb$^+_2$	366.3 (6.00)	475 (14)	0.030
2Hg^{2+}	377.4 (5.54)	464 (3)	0.0076
2Hg$^{2+}_2$	387.6; 409.8 (4.24; 4.31)	530 (69)	0.0024
2H$^+$	382; 433 (4.16; 4.06)	549 (88)	0.0064
2H$^+_2$	458.7 (5.54)	549 (88)	0.0015

[a] Wavelengths of absorption maxima and molar absorption coefficients (M^{-1} cm^{-1}) in parentheses. [b] Wavelengths of maxima in fluorescence spectra and shifts $\Delta\lambda = \lambda_C - \lambda_L$ (subscripts L and C designate ligand and complex, respectively). [c] Fluorescence quantum yields.

The effect of oxygen on fluorescence intensity was evaluated at 25 °C for the free ligand **2** (5×10^{-5} M in AN) and for its complexes with Ba^{2+} (with [**2**] = 2×10^{-5} M, $[Ba^{2+}] = 5 \times 10^{-5}$ M) and Mg^{2+} (with [**2**] = 2×10^{-5} M, $[Mg^{2+}] = 2 \times 10^{-5}$ M). Comparison of Ar and air saturated solutions revealed a very small decrease in fluorescence intensity in all three cases. A more reliable measure of the oxygen effect was obtained from the ratios of intensities of Ar- and O_2-outgassed solutions. Assuming diffusion controlled quenching by oxygen ($k_{qox} = 3.5 \times 10^{10}$ M^{-1} s^{-1})[29] and $[O_2] = 9.1 \times 10^{-3}$ M[30] gives fluorescence lifetimes (τ_f) of 0.23, 0.46, and 0.26 ns for free ligand **2** and its complexes with Ba^{2+} (mainly 2:2) and Mg^{2+} (mainly 1:1), respectively. To the extent that these observations can be generalized, they show that the use of air-saturated solutions should lead to minor attenuations in the quantum yield values (2−3%). The roughly 2-fold increase in the fluorescence lifetime of **2$_2$·(Ba^{2+})$_2$** relative to the free ligand accounts for part of the 3-fold increase in its fluorescence quantum yield. Complexation with both Ba^{2+} and Mg^{2+} appears to lead to a modest increase in the radiative rate constant (note the 2-fold increase of the quantum yield of the Mg^{2+} complex relative to **2** in the absence of significant change in the lifetime). Comparison of the free ligand fluorescence quantum yield with that of the **2$_2$·(Ba^{2+})$_2$** complex is not straightforward because their lifetimes are dominated by entirely different photochemical events. In the free ligand (and in complexes whose structure does not restrict torsional relaxation), the main radiationless process is torsional relaxation leading to trans → cis photoisomerization, whereas in the 2:2 complex that decay channel is entirely suppressed and is replaced by intramolecular bond formation leading to ligand photodimers.

Shifts in the fluorescence spectra on complexation are given in Table 2. The λ^{fl}_{max} values of the fluorescence spectra of 1:1 complexes, **2·M^{n+}**, with alkali and alkaline earth metal cations are nearly identical with that of the free ligand **2**. Fluorescence spectra of complexes with 2:2 stoichiometry, **2$_2$·(M^{n+})$_2$**, generally show small red shifts in λ^{fl}_{max} in contrast to the blue shifts in the λ_{max} of the corresponding absorption spectra. This result suggests excitonic interaction between the chromophores in the sandwich pair with λ_{max} in absorption assigned to the blue shifted allowed pair state and λ^{fl}_{max} assigned to the lower lying

forbidden pair state. No obvious trend is observed in λ_{max}^{fl} shifts of 1:2 complexes, $\mathbf{2 \cdot (M^{n+})_2}$.

Conclusions

The multitopic receptor **2**, a bis(crown ether) distyryl heterocyclic molecule, was synthesized and its ability to form complexes with several metal cations was evaluated. Complex formation with alkali and alkaline earth cations results in similar changes in absorption and fluorescence spectra as were observed in the parallel study of mono(crown ether) analogue **1**.[8] The changes depend on the stoichiometry of the complex and on the site of complexation. Complexes of 2:2 stoichiometry ($\mathbf{2_2 \cdot (M^{n+})_2}$) involving cation binding at the crown ether moieties have sandwich structures and exhibit spectral changes consistent with excitonic coupling of transition dipole moments: somewhat weaker absorbance with a hypsochromic shift in the λ_{max} of the UV spectrum and development of a weak shoulder at the onset of the spectrum, consistent with a bathochromic shift in the fluorescence spectrum. Alternatively, the development of the shoulder in the absorption spectrum could reflect the structural heterogeneity of the complex. Complexes involving alkali and alkaline earth cations bound at the crown ether moiety(ies) of a single ligand **2** ($\mathbf{2 \cdot M^{n+}}$ or $\mathbf{2 \cdot (M^{n+})_2}$) exhibit enhanced absorbances and smaller hypsochromic shifts in the λ_{max} of the UV spectrum. With some exceptions, corresponding changes in the fluorescence spectra on complex formation of **2** also parallel those observed for **1**.[8] Generally, smaller λ_{max}^{fl} shifts are observed for single ligand complexes of **2** than of **1**: compare 46 and 42 nm blue shifts on complexation of **1** with one Mg^{2+} or Ca^{2+}, respectively,[8] with essentially no shift on complexation with **2**. For both ligands, coordination with Hg^{2+} leads to pronounced red shifts in λ_{max} of absorption and fluorescence spectra, which are similar to those observed on protonation suggesting binding at the N atoms of the heterocyclic moieties. Such binding is associated with attenuated fluorescence intensity, in contrast to binding to the crown ether moieties, which leads to enhanced fluorescence intensity.

Sandwich complexes of **1** and **2** are associated with large stability constants and are favored at low cation concentrations. Of the metal cations studied, complexes of **2** with K^+ and Ba^{2+} exhibit the largest stability constants in their respective groups indicating that **2** has potential as a selective optical sensor for these ions.

Acknowledgment. This work was supported by the CRDF (Grant RC2-2344-MO-02 jointly awarded to M.A. and J.S.), the RFBR (Project 03-03-32849), and the Integration Program (Ministry of High Education of Russia). At Florida State University it was supported, in part, by the National Science Foundation (Grant CHE 0314784 to J.S.).

References and Notes

(1) Valeur, B.; Badaoui, F.; Bardez, E.; Bourson, J.; Boutin, P.; Chatelein, A.; Devol, I.; Larrey, B.; Lefevre, J. P.; Soulet, A. In *Chemosensors of Ion and Molecular Recognition*; Desvergne, J.-P., Czarnik, A. W., Eds.; NATO ASI Series; Kluwer: Dordrecht, The Netherlands, 1977; p 195.

(2) Rettig, W.; Lapouyade, R. In *Topics in Fluorescence Spectroscopy*; Lakowics, J. R., Ed.; Plenum: New York, 1994; Vol. 4, p 109.

(3) De Silva, A. P.; Gunaratne, H. Q. N.; Gunnlaugsson, T.; Huxley, A. J. M.; McCloy, C. P.; Rademacher, J. T.; Rice, T. E. *Chem. Rev.* **1997**, *97*, 1515.

(4) Valeur, B.; Leray, I. *Coord. Chem. Rev.* **2000**, *205*, 3.

(5) Alfimov, M.; Fedorova, O.; Gromov, S. *Photochem. Photobiol. A* **2003**, *158*, 183−198.

(6) Fedorova, O.; Andryukhina, E.; Gromov, S. *Synthesis* **2003**, *4*, 593−597.

(7) Fedorov, Yu.; Fedorova, O.; Gromov, S.; Bobrovsky, M.; Andryukhina, E.; Alfimov, M. *Russ. Chem. Bull.* **2002**, *51*, 789−795.

(8) Fedorov, Yu. V.; Fedorova, O. A.; Andryukhina, E. N.; Gromov, S. P.; Alfimov, M. V.; Kuzmina, L. G.; Churakov, A. V.; Howard, J. A. K.; Aaron, J.-J. *New J. Chem.* **2003**, *27*, 280−288.

(9) Kimura, K.; Yokota, G.; Yokoyama, M.; Uda, R. M. *Macromolecules* **2001**, *34*, 2262−2268.

(10) Inoue, Y.; Hakushi, T.; Liu, Y.; Tong, L.; Hu, J.; Zhao, G.; Huang, Sh.; Tian, B. *J. Phys. Chem.* **1988**, *92* (8), 2371−2374.

(11) Liu, Y.; Tong, L. H.; Huang, Sh.; Tian, B. Zh.; Inoue, Y.; Hakushi, T. *J. Phys. Chem.* **1990**, *94* (6), 2666−2670.

(12) An, H. Y.; Bradshaw, J. S.; Izatt, R. M.; Yan. Z. M. *Chem. Rev.* **1994**, *94* (4), 939−991.

(13) Hansson, A. P.; Norrby, P.-O.; Warnmark, K. *Tetrahedron Lett.* **1998**, *39*, 4565−4568.

(14) Yamamoto, K.; Yumioka, H.; Okamoto, Y.; Chikamatsu, H. *J. Chem. Soc., Chem. Commun.* **1987**, 168−169.

(15) Lindsten, G.; Wennerstrom, O.; Thulin, B. *Acta Chem. Scand.* **1986**, *B40*, 545−554.

(16) Shinkai, S.; Ogawa, T.; Nakaji, T.; Manabe, O. *J. Chem. Soc., Chem. Commun.* **1980**, 373.

(17) Marcotte, N.; Fery-Forgues, F.; Lavabre, D.; Marguet, S.; Pivovarenko, V. G. *J. Phys. Chem. A* **1999**, *103*, 3163.

(18) Xia, W.-S.; Schmehl, R. H.; Li, C.-J.; Mague, J. T.; Luo, C.-P.; Guldi, D. M. *J. Phys. Chem. B* **2002**, *106*, 833−843.

(19) Kiprianov, A. I.; Mikhailenko F. A. *Him. Heterocycl. Soed.* **1967**, 270.

(20) Green, A.; Perkin, A. *J. Chem. Soc.* **1903**, *33*, 1201.

(21) (a) Melhuish, W. H. *J. Phys. Chem.* **1960**, *64*, 762−764. (b) Demas, J. N.; Crosby, G. A. *J. Phys. Chem.* **1971**, *75*, 991−1024.

(22) Meech, S. R.; Phillips, D. *J. Photochem.* **1983**, *23*, 193−217.

(23) (a) Gans, P.; Sabatini, A.; Vacca, A. *Talanta* **1996**, *43*, 1739. (b) Alfimov, M. V.; Gromov, S. P.; Fedorov, Yu. V.; Fedorova, O. A.; Vedernikov, A. I.; Churakov, A. V.; Kuz'mina, L. G.; Howard, J. A. K.; Bossmann, S.; Braun, A.; Woerner, M.; Sears, D. F., Jr.; Saltiel, J. *J. Am. Chem. Soc.* **1999**, *121*, 4992−5000. (c) Fedorova, O. A.; Fedorov, Yu. V.; Vedernikov, A. I.; Gromov, S. P.; Yescheulova, O. V.; Alfimov, M. V.; Woerner, M.; Bossmann, S.; Braun, A.; Saltiel, J. *J. Phys. Chem. A* **2002**, *106*, 6213−6222

(24) Fedorov, Yu. V.; Fedorova, O.; Schepel, N.; Alfimov, M.; Saltiel, J. Unpublished observations.

(25) For relevant applications see: (a) Zimányi, L.; Kulcsár, Á.; Lanyi, J. K.; Sears, D. F., Jr.; Saltiel, J. *Proc. Natl. Acad. Sci. U.S.A.* **1999**, *96*, 4408−4413. (b) Zimányi, L.; Kulcsár, Á.; Lanyi, J. K.; Sears, D. F., Jr.; Saltiel, J. *Proc. Natl. Acad. Sci. U.S.A.* **1999**, *96*, 4414−4419. (c) Kulcsár, Á.; Saltiel, J.; Zimányi, L. *J. Am. Chem. Soc.* **2001**, *123*, 3332−3340.

(26) (a) Lawton, W. H.; Sylvestre, E. A. *Technometrics* **1971**, *13*, 617−633. (b) Sylvestre, E. A.; Lawton, W. H.; Maggio, M. S. *Technometrics* **1974**, *16*, 353−368.

(27) Kasha, M.; Rawls, H. R.; El-Bayoumi, M. A. *Pure Appl. Chem.* **1965**, *11*, 371−392.

(28) Catalán, J.; Zimányi, L.; Saltiel, J. *J. Am. Chem. Soc.* **2000**, *122*, 2377−2378.

(29) Saltiel, J.; Krishnamoorthy, G.; Huang, Z.; Ko, D.-H.; Wang, S. *Can. J. Chem.* **2003**, *81*, 673−679.

(30) Clark, W. D. K.; Steel, C. *J. Am. Chem. Soc.* **1971**, *93*, 6347−6355.